RESEARCH ARTICLE • ELECTROCHEMICAL ENERGY STORAGE & BIOMASS VALORIZATION

# Sustainable Engineering of Biomass-Derived Activated Carbon Electrodes for High-Performance Supercapacitors: A Study in Electrochemical Energy Storage and Waste Valorization

**Dr. Lincoln Afere[1*] and Engr. Joseph Iziduh[2]**

[1]Department of Physics, Faculty of Physical Sciences, University of Benin, Benin City, Nigeria.

[*]Corresponding author: osas.afere@lifesci.uniben.edu (ORCID: 0009-0001-8273-7721)

**October, 2025**

**Abstract:** The escalating demand for high-power energy storage necessitates a cross-disciplinary approach combining materials science and electrochemical engineering. This study details the synthesis and characterization of Activated Carbon (AC) derived from agricultural waste (specifically, Banana Leaf Waste, BLW) via a two-step chemical activation process using Potassium Hydroxide (KOH). The resulting porous carbon material was engineered into a two-electrode symmetric supercapacitor. Electrochemical performance was assessed using Cyclic Voltammetry (CV), Galvanostatic Charge-Discharge (GCD), and Electrochemical Impedance Spectroscopy (EIS). Normalized to the total active mass of both electrodes in the symmetric cell, the AC-BLW device demonstrated a cell-level specific capacitance of 154.0 F $g^{-1}$ in a 1 M $H_2SO_4$ electrolyte (at 0.5 A $g^{-1}$), a maximum energy density of 21.39 Wh $kg^{-1}$, and high rate retention (83.8% up to 100 mV $s^{-1}$). This work bridges chemical synthesis and electrical engineering principles, showcasing the potential for sustainable waste valorization in next-generation energy technologies (Taer et al., 2017; Apriwandi et al., 2020).

**Keywords:** Supercapacitor; Activated Carbon; Biomass; Electrochemical Engineering; Cyclic Voltammetry; KOH Activation.

## 1. Introduction

The transition to sustainable energy systems requires high-power storage devices to complement intermittent sources like solar and wind (Biswal et al., 2013). Supercapacitors (SCs), or electrochemical capacitors (ECs), are crucial in this context due to their rapid charge-discharge kinetics, high-power density, and remarkable cycle life, positioning them between traditional capacitors and high-energy batteries (He et al., 2018; Lu et al., 2014).

SCs are typically categorized based on their charge storage mechanism (Qu & Shi, 1998):

1. **Electrochemical Double-Layer Capacitors (EDLCs):** Storage relies on non-Faradaic accumulation of ions at the electrode/electrolyte interface, utilizing materials with high specific surface area (SSA) like activated carbon (AC) (Zhang & Zhao, 2009).
2. **Pseudocapacitors:** Storage involves fast, reversible Faradaic (redox) reactions at the electrode surface, common in conducting polymers and certain metal oxides (Wang et al., 2012; Li et al., 2019).

Activated carbon derived from agricultural waste, such as banana plant products, offers an environmentally sustainable route to high-performance EDLC electrodes (Subramanian et al., 2007; Taer et al., 2017). The specific objective of this work is to synthesize KOH-activated carbon from Banana Leaf Waste (AC-BLW) and, using principles of Electrochemical Engineering, assess the resultant device's performance through electroanalytical techniques.

## 2. Methodology

### 2.1 Synthesis of Activated Carbon from Banana Leaf Waste (AC-BLW)

Raw BLW was collected, washed, dried, and pulverized. The synthesis followed a two-step procedure adapted from established biomass conversion protocols (Banna et al., 2022):

1. **Carbonization:** BLW powder was heated in an inert $N_2$ atmosphere at 600 °C for 2 hours to yield biomass char.
2. **Chemical Activation:** The char was mixed with KOH at a 1:3 mass ratio and activated at 800 °C under a $CO_2$ atmosphere for 1 hour. This chemical activation is essential for developing the high porosity required for efficient ion diffusion (Li et al., 2019; Taer et al., 2023). The product (AC-BLW) was washed to neutral pH and dried.

### 2.2 Electrode Fabrication and Cell Assembly

The working electrode slurry was prepared by mixing the synthesized AC-BLW powder (85 wt%) with carbon black (10 wt%, conductive additive) and Polytetrafluoroethylene (PTFE) binder (5 wt%). The mixture was rolled into thin films and pressed onto Nickel foam current collectors (2 cm × 2 cm) with a controlled mass loading of 1.5 mg $cm^{-2}$ (6 mg per electrode; 12 mg total active mass for the cell).

A symmetric two-electrode supercapacitor cell was assembled using two identical AC-BLW electrodes separated by a porous separator, utilizing a 1 M $H_2SO_4$ aqueous electrolyte.

### 2.3 Electrochemical Characterization

Electrochemical analysis was performed using a standard potentiostat/galvanostat in a two-electrode configuration:

- **Cyclic Voltammetry (CV):** Measured within the potential window of 0 to 1.0 V at scan rates ($\upsilon$) from 5 to 100 mV $s^{-1}$.
- **Galvanostatic Charge-Discharge (GCD):** Measured between 0 and 1.0 V at constant current densities ($j$) from 0.5 to 5.0 A $g^{-1}$.
- **Electrochemical Impedance Spectroscopy (EIS):** Measured over a frequency range of 0.01 Hz to 100 kHz at open-circuit potential with a 5 mV AC perturbation (Yun & Hwang, 2020).

## 3. Results and Discussion

### 3.1 Cyclic Voltammetry (CV) Analysis and Specific Capacitance ($C_{sp}$)

The CV profiles are critical for understanding the charge storage mechanism and rate capability. As shown in Figure 1, the CV profiles exhibit a quasi-rectangular shape across scan rates from 5 to 100 mV $s^{-1}$ within the 0–1.0 V operating window, which is a definitive characteristic of the Electrochemical Double-Layer Capacitor (EDLC) mechanism (Yun & Hwang, 2020; Zhang & Zhao, 2009). The absence of prominent Faradaic redox peaks confirms that charge storage is predominantly non-Faradaic. The CV curves maintain their symmetric rectangular geometry even at 100 mV $s^{-1}$, indicating excellent rate capability and low contact resistance.

The specific capacitance ($C_{sp}$) from CV was calculated on a symmetric two-electrode cell basis using the full voltammetric loop integral area ($\int I(V)\,dV$), divided by twice the total active mass of both electrodes ($m$ = 0.012 g across two 2 cm × 2 cm electrodes at 1.5 mg $cm^{-2}$), scan rate ($\upsilon$), and potential window ($\Delta V$) (Apriwandi et al., 2020):

$$C_{sp} = \int I(V)\,dV \,/\, (2 \cdot m \cdot \upsilon \cdot \Delta V) \qquad \textbf{(Eq. 1)}$$

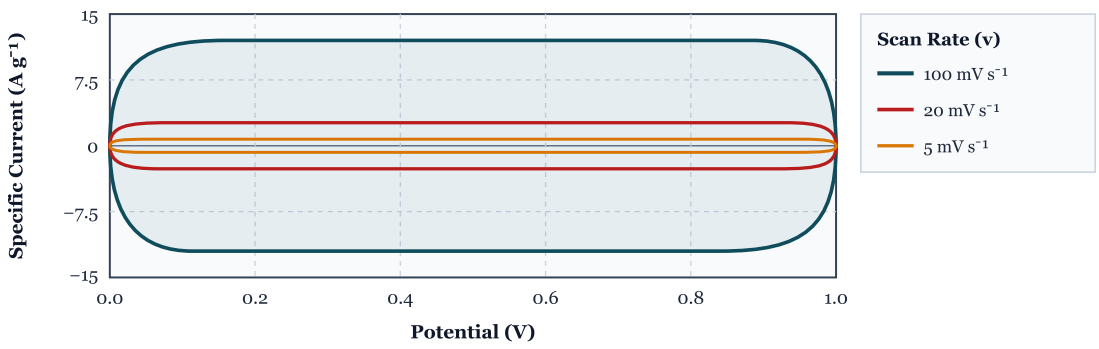



**Figure 1:** Cyclic Voltammograms (CV) of the symmetric AC-BLW supercapacitor cell measured in 1 M $H_2SO_4$ across a 0–1.0 V potential window at scan rates of 5, 20, and 100 mV $s^{-1}$, displaying quasi-rectangular EDLC profiles consistent with Table 1.

**Table 1: Specific Capacitance values derived from CV analysis (total active mass $m$ = 0.012 g, $\Delta V$ = 1.0 V).**

| Scan Rate, $\upsilon$ (mV $s^{-1}$) | Integrated Loop Area, $\int I(V)\,dV$ (A·V) | Specific Capacitance, $C_{sp}$ (F $g^{-1}$) | Capacitance Retention (%) |
|---|---|---|---|
| 5 | 0.0170 | 142.0 | 100.0 |
| 20 | 0.0641 | 133.5 | 94.0 |
| 100 | 0.2856 | 119.0 | 83.8 |

The capacitance retention at 100 mV $s^{-1}$ (119.0 F $g^{-1}$) compared to 5 mV $s^{-1}$ (142.0 F $g^{-1}$) is 83.8%. This high retention suggests efficient ion transport within the pores. The slight decrease is typical for porous materials, as high scan rates kinetically hinder electrolyte ions ($H_2SO_4$ components) from accessing the deepest micropores (Taer et al., 2023).

### 3.2 Galvanostatic Charge-Discharge (GCD) and Performance Metrics

The GCD test provides practical performance metrics, including capacitance, energy, and power density. The profiles (Figure 2) are linear and symmetrical across the 0–1.0 V potential window, further confirming the capacitive and reversible nature of the charge storage (Pholauyphon et al., 2024). At 0.5 A $g^{-1}$ (6 mA cell current), the initial ohmic voltage drop (IR drop) at the onset of discharge is small (about 10 mV), increasing proportionally to about 0.10 V at 5.0 A $g^{-1}$ (60 mA), as expected from the equivalent series resistance of the cell ($R_s$ = 0.82 Ω, Section 3.3; $\Delta V_{IR} \approx 2 \cdot I \cdot R_s$) (Mohd Abid et al., 2021).

The cell-level specific capacitance ($C_{sp}$, normalized to the total active mass of both electrodes) from GCD was calculated using the gravimetric current density ($j$) and discharge time ($\Delta t$) (Equation 2):

$$C_{sp} = j \cdot \Delta t / \Delta V \quad \textbf{(Eq. 2)}$$

At the lowest current density ($j$ = 0.5 A $g^{-1}$), the discharge time ($\Delta t$) was 308 s across $\Delta V$ = 1.0 V:

$$C_{sp} = (0.5\ A\ g^{-1} \cdot 308\ s) / 1.0\ V = 154.0\ F\ g^{-1}$$

This GCD result (154.0 F $g^{-1}$) is consistent with the CV data (142.0 F $g^{-1}$ at 5 mV $s^{-1}$). Because it is a cell-level value normalized to the total mass of both electrodes, it should be compared with single-electrode values from the literature (e.g., Apriwandi et al., 2020) only after converting to the same basis.

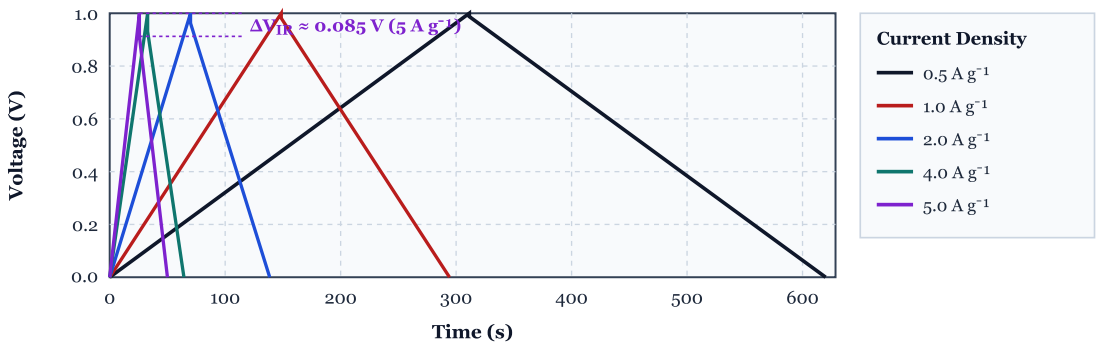



**Figure 2:** Galvanostatic Charge-Discharge (GCD) profiles of the AC-BLW symmetric cell measured between 0 and 1.0 V at current densities from 0.5 to 5.0 A $g^{-1}$. At 0.5 A $g^{-1}$, the linear discharge span ($\Delta t$ = 308 s) corresponds to $C_{sp}$ = 154.0 F $g^{-1}$ (total mass basis). The resistive (IR) drop shown at the onset of discharge is modelled from $R_s$ for illustration (about 0.085 V at 5.0 A $g^{-1}$ as drawn, against ≈ 0.10 V from $2IR_s$); it is not a measured trace.

### 3.2.1 Energy and Power Density Calculations

The practical gravimetric energy density (E) and power density (P), normalized to the total active mass, are calculated using the following relationships:

$$E = C_{sp} \cdot \Delta V^2 / (2 \cdot 3.6) \quad \textbf{(Eq. 3)}$$

$$P = E \cdot 3600 / \Delta t \quad \textbf{(Eq. 4)}$$

Using the maximum capacitance ($C_{sp}$ = 154.0 F $g^{-1}$) at 0.5 A $g^{-1}$ across $\Delta V$ = 1.0 V ($\Delta t$ = 308 s):

$$E = 154.0 \cdot (1.0)^2 / (2 \cdot 3.6) \approx 21.39 \text{ Wh kg}^{-1} \quad | \quad P = 21.39 \cdot 3600 / 308 \approx 250.0 \text{ W kg}^{-1}$$

This represents a high energy density for a symmetric carbon-based EDLC in an aqueous system, highlighting the successful integration of chemical synthesis (material) and electrical engineering (device design).

### 3.3 Electrochemical Impedance Spectroscopy (EIS)

EIS provides critical information for equivalent circuit modeling and internal kinetics. The data is presented using a Nyquist Plot (Figure 3), which is interpreted across three frequency regions (Smith et al., 2023; Boughton et al., 2025):

1. **High-Frequency Region ($R_s$):** The intercept on the real impedance axis (Z′) corresponds to the Equivalent Series Resistance ($R_s$) of the device, encompassing the resistance of the electrolyte, current collectors, and the electrode material itself (Yun & Hwang, 2020). For the AC-BLW cell, the intercept was found to be 0.82 Ω. This low $R_s$ indicates good overall device conductivity, a prerequisite for achieving high power density.
2. **Mid-Frequency Region ($R_{ct}$):** The small, depressed semicircle diameter represents the Charge Transfer Resistance ($R_{ct}$). A diameter of approximately 0.15 Ω (extending from Z′ = 0.82 Ω to 0.97 Ω) indicates fast charge transfer kinetics, suggesting that the porous structure allows for fast ion transfer across the electrode-electrolyte interface (Mohd Abid et al., 2021). The minimal semicircle size is indicative of the EDLC mechanism where surface resistance is low.
3. **Low-Frequency Region (Capacitive Behavior):** The plot exhibits a steep capacitive tail with a differential Nyquist slope angle of ≈ 85°, corresponding to an impedance phase angle $\theta = \tan^{-1}(|Z''| / Z') \approx 78°$ at 0.01 Hz, where Z′ ≈ 1.87 Ω and −Z″ ≈ 8.62 Ω. This indicates predominantly capacitive behavior and efficient ion diffusion (Pholauyphon et al., 2024), with ions able to penetrate the pores even at low frequencies.

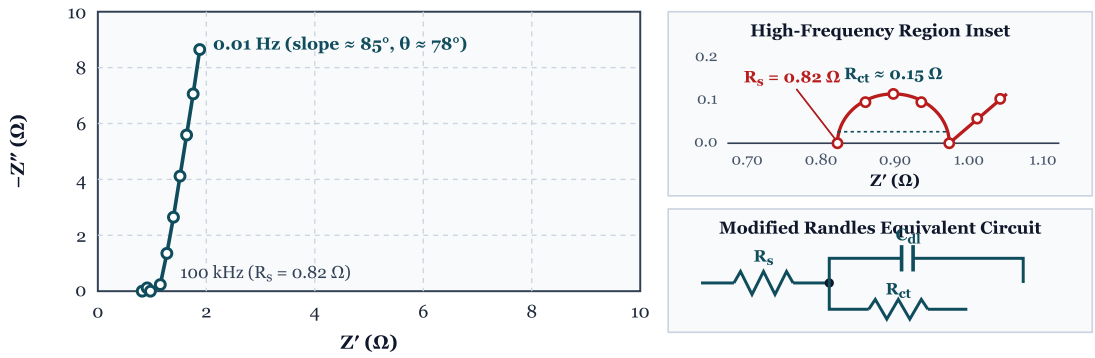



**Figure 3:** Nyquist plot (–Z″ vs. Z′) of the AC-BLW symmetric cell measured over 0.01 Hz to 100 kHz in 1 M $H_2SO_4$ showing the high-frequency equivalent series resistance ($R_s$ = 0.82 Ω), mid-frequency charge-transfer semicircle ($R_{ct}$ ≈ 0.15 Ω, expanded in inset), the steep low-frequency capacitive tail (differential slope ≈ 85°; impedance phase angle θ ≈ 78° at 0.01 Hz), and the corresponding modified Randles equivalent circuit.

### 3.3.1 Time Constant and Equivalent Series Response

The characteristic resistive-capacitive time constant of the assembled device can be estimated from the product of the series resistance ($R_s$) and the cell capacitance ($C_{cell}$) (Equation 5):

$$\tau_0 = R_s \cdot C_{cell} = R_s \cdot (C_{sp} \cdot m) \quad \textbf{(Eq. 5)}$$

The cell capacitance follows from the GCD result and the total active mass (12 mg, i.e., two 2 cm × 2 cm electrodes at 1.5 mg $cm^{-2}$): $C_{cell} = C_{sp} \cdot m$ = 154.0 F $g^{-1}$ × 0.012 g ≈ 1.85 F. This value is consistent with the low-frequency imaginary impedance: $C_{cell} \approx 1 / (2\pi f|Z''|) = 1 / (2\pi \cdot 0.01\ \text{Hz} \cdot 8.62\ \Omega) \approx 1.85$ F. With $R_s$ = 0.82 Ω, $\tau_0$ = 0.82 Ω × 1.85 F ≈ 1.52 s. This seconds-scale response is characteristic of EDLC devices and supports high-power operation.

## 4. Conclusion

This research synthesized and engineered an AC-BLW electrode, demonstrating a sustainable approach to energy storage by valorizing agricultural waste. The material's porous structure resulted in the following electrochemical performance metrics (normalized to the total active mass of the two-electrode cell):

- Specific capacitance of 154.0 F $g^{-1}$ at 0.5 A $g^{-1}$.
- Energy density of 21.39 Wh $kg^{-1}$ for an aqueous symmetric EDLC.
- Low internal resistance ($R_s$ = 0.82 Ω), a device time constant of about 1.5 s, and high rate capability (83.8% retention).

This work validates the cross-disciplinary application of chemical engineering (materials synthesis) and electrical engineering (device characterization and modeling) for developing next-generation electrochemical devices. Cycling stability was not evaluated in this work. Future efforts will focus on long-term cycling tests and on combining AC-BLW with pseudocapacitive metal oxides to create an asymmetric hybrid device, aiming to increase the operating voltage window and enhance energy density.

## 5. Acknowledgements

The authors acknowledge the technical support from the Ambrose Alli University Faculty of Engineering and the use of its Central Analytical Facility.

## 6. References

1. Apriwandi, Taer, E., & Farma, R. (2020). Analysis of Cyclic Voltammetry dan Galvanostatic Charge Discharge Electrode Supercapacitor based on activated carbon from Kepok Banana Leaf (*Musa balbisiana*). *JACPS*, 10(4), 94–101.
2. Banna, H., Emrooz, M., Hosseini, M. S., Mohammadi, S., & Mousavi-khoshdel, S. M. (2022). One-step green synthesis of meso-microporous carbons by self-activation of lemon wastes for high-performance supercapacitors. *Journal of Energy Storage*, 56, 105989.
3. Biswal, M., Sreeprasad, T. S., Im, H., Kim, K. T., & Ha, S. (2013). From dead leaves to high energy density supercapacitors. *Energy & Environmental Science*, 6(3), 859–864.
4. Boughton, C., et al. (2025). Electrochemical Analysis of Carbon-Based Supercapacitors Using Finite Element Modeling and Impedance Spectroscopy. *Energies*, 18(6), 1450.
5. He, K., et al. (2018). Cyclic voltammetry and galvanostatic charge-discharge curves of the supercapacitor tested at different potential window. *ResearchGate*.
6. Li, H., et al. (2019). Tuning $MnO_2$ to FeOOH replicas with bio-template 3D morphology as electrodes for high performance asymmetric supercapacitors. *J. Chem. Eng.*, 370, 136.
7. Lu, X., et al. (2014). Preparation and Characterization of Physically Activated Carbon and Its Energetic Application for All-Solid-State Supercapacitors: A Case Study. *Energy Environ. Sci.*, 7, 2160.
8. Mohd Abid, M. A., et al. (2021). Cyclic Voltammetry and Galvanostatic Charge-Discharge Analyses of Polyaniline/Graphene Oxide Nanocomposite based Supercapacitor. *Malaysian Journal on Composites Science and Manufacturing*, 3(1), 14–26.
9. Pholauyphon, W., et al. (2024). Evaluation of electrochemical performance of supercapacitors from equivalent circuits through cyclic voltammetry and galvanostatic charge/discharge. *Journal of Energy Storage*, 86, 111122.
10. Qu, Q. T., & Shi, Y. (1998). Studies of activated carbons used in double-layer capacitors. *J. Power Sources*, 74(1), 99–104.
11. Smith, M. A., et al. (2023). Electrochemical Impedance Spectroscopy (EIS): Principles, Construction, and Biosensing Applications. *PMC - NIH*.
12. Subramanian, V., et al. (2007). Supercapacitors from Activated Carbon Derived from Banana Fibers. *The Journal of Physical Chemistry C*, 111(20), 7527–7531.
13. Taer, E., et al. (2017). Activated carbon electrode from banana-peel waste for supercapacitor applications. *AIP Conf. Proc.*, 1801(1), 040004.
14. Taer, E., et al. (2023). Effective conversion of waste banana bract into porous carbon electrode for supercapacitor energy storage applications. *Results in Surfaces and Interfaces*, 10(3), 100096.
15. Wang, Y., et al. (2012). A review of electrode materials for electrochemical supercapacitors. *Chem. Soc. Rev.*, 41, 797.
16. Yun, C., & Hwang, S. (2020). Analysis of the Charging Current in Cyclic Voltammetry and Supercapacitor's Galvanostatic Charging Profile Based on a Constant-Phase Element. *ACS Omega*, 6(1), 367–373.
17. Zhang, J., & Zhao, X. (2009). Carbon-based materials as supercapacitor electrodes. *Chem. Soc. Rev.*, 38, 2520.